RSC Advances

PAPER

View Article Online
View Journal | View Issue

Cite this: *RSC Adv.*, 2020, **10**, 11210

Fabrication of high B-doped ordered mesoporous carbon with 4-hydroxyphenylborate phenolic resin for supercapacitor electrode materials†

Yan Zhang, * Fengsong Qi and Yujian Liu

Received 18th January 2020
Accepted 10th March 2020

DOI: 10.1039/d0ra00561d

rsc.li/rsc-advances

The high B-doped ordered mesoporous carbon (HPB-OMC) was prepared by using 4-hydroxyphenylboronic acid-modified phenolic resin (HPBPF) as a boron and carbon precursor *via* the evaporation-induced self-assembly (EISA) approach. The chemical composite, mesoporous structure, and electrochemical properties of the as-prepared HPB-OMC are investigated. The results show that both highly boron-doped and well-ordered mesoporous structure are achieved for HPB-OMCs, owing to the improvement of solubility of the resins in ethanol, and the enhancement of thermal stability of pore channels during carbonization. Moreover, the HPB-OMCs exhibit an ideal electric double-layer capacitor performance. With the increase of the B-doped content, the specific capacitance of the HPB-OMC electrode rises gradually, then drops off a little. The HPB-OMC with a high B content (3.96 wt%) shows a much high specific capacitance of 183 F g^{-1} at a current density of 1 A g^{-1}, suggesting its promising application in the field of supercapacitors.

1. Introduction

Ordered mesoporous carbons (OMCs) have been widely applied in catalytic reactions,[1,2] lithium-ion batteries,[3,4] supercapacitors,[5,6] CO_2 adsorption,[7,8] biomedicines,[9] *etc.*, owing to large pore volume and high specific surface area. Furthermore, heteroatoms like N,[1] B,[10] and P[11] have been doped into mesoporous carbon materials to improve their reactivity. Among them, electron deficient-boron doping can decrease the Fermi energy level of carbon material, regulate oxygen chemisorption and oxidation–reduction reaction to obtain pseudo capacitance in the supercapacitor.[12,13] The boron-doped OMCs show a high potential application in the field of supercapacitors.

Many techniques have been attempted to prepare boron-doped ordered mesoporous carbons (B-OMCs). For example, Lee[14] obtained B-OMCs by using SBA-15 as the hard template, sucrose and boric acid as the precursor. The boron content of B-OMCs increases to 2.11 at% by co-impregnating SBA-15 temple with sucrose and 4-hydroxyphenylboronic acid. As a metal-free ORR catalyst, the obtained B-OMCs show high electrocatalytic activity, anti-methanol toxicity, and chemical stability.[15] Compared with the multistep and cost hard template, the evaporation induced self-assembly (EISA) is more efficient, and become the primary method for the preparation of B-OMCs. Zhao[16] synthesized B-OMCs by boron-modified phenolic resin (BPF). Nevertheless, when the boron content exceeded 1.01 wt%, the specific surface area of B-OMCs decreased from 462 to 314 m^2 g^{-1}. Moreover, other atoms like nitrogen,[17] cobalt[18] have also been co-doped with boron to improve OMCs further. The properties and preparation method of B-OMCs are listed in Table 1.

Most of the research focuses on using boric acid as the boron source, and phenol-formaldehyde resin or resorcinol-formaldehyde resin as the carbon precursor. The solubility of BPF decreases with the reaction of boric acid and hydroxyl of phenolic resins, so to affect the self-assembly process. It is still a challenge to balance the high boron-doped content and well-ordered mesoporous structure.

The thermal stability of the phenolic resins could be enhanced obviously by the introduction of phenylboronic acid into the backbone because oxygen atom bonded with boron atoms in phenylboronate did not participate in the formation of volatile carbon oxides during pyrolysis.[23] And the char yield of the modified resins rises to 76.2% at 800 °C.[24]

In this paper, the new boron-doped mesoporous carbons (HPB-OMCs) were successfully fabricated by using 4-hydroxyphenylboronic acid-modified phenolic resin as the precursors *via* evaporation-induced self-assembly (EISA). The phenolic hydroxyl of 4-hydroxyphenylboronic acid could improve the solubility of the resin. And the high thermal stability of the

Key Laboratory of Specially Functional Polymeric Materials and Related Technology (ECUST), Ministry of Education, School of Materials Science and Engineering, East China University of Science and Technology, Mei Long Road 130, Shanghai 200237, PR China. E-mail: yzhang@ecust.edu.cn; Fax: +86 21 64252659; Tel: +86 21 64252394

† Electronic supplementary information (ESI) available. See DOI: 10.1039/d0ra00561d

Table 1 The properties and preparation methods of B-OMCs

Precursors			Property			
Boron	Carbon	Methods	B content	S_{BET} (m^2 g^{-1})	Specific capacitance	Ref.
Boric acid	Sucrose	Hard template	—	848–1337	—	14
Boric acid	Phenolic resins	EISA	1.01–1.35 wt%	314–462	0.38–0.39 F m^{-2} (current density: 0.2 A g^{-1}, three-electrode)	16
Boric acid	Sucrose	Hard template	0.2–0.6 wt%	470–660	0.21 F m^{-2} (potential sweep rate: 2 mV s^{-1}, interfacial capacitance)	18
Boric acid	Resorcinol	EISA	0.42–2.37 at%	547–643	156 F g^{-1} (current density: 1 A g^{-1}, three-electrode system)	19
Boric acid	Phenolic resins	EISA	1.10–1.26 wt%	330–620	180 F g^{-1} (current density: 0.1 A g^{-1}, three-electrode system)	20
Boric acid	Phenolic resins	One-pot synthesis	0.75–1.77 wt%	470–626	Enhance the electrocatalytic activity of oxygen reduction reaction	21
Boric acid	Phenolic resins	EISA	1.69–1.96 wt%	122–690	200 F g^{-1} (current density: 0.2 A g^{-1}, three-electrode system)	22
4-Hydroxyphenylboronic acid	Phenolic resins	Hard template	0.41–1.36 at%	131–468	Efficient non-metal oxygen reduction reaction catalysts	15

resin is beneficial to reduce shrinkage of the channel during pyrolysis to obtain a well-ordered mesoporous structure. Besides, more B–C σ bonds are retained in the lattice of the carbons. Because of the larger electronegativity of carbon concerning boron, B–C bonds are polarized considerably. The positive charge (0.56*e*) on the boron atom is conducive to the capture of the O_2 molecule,[25] leading to the pseudo capacitance of mesoporous carbon increasing. The effect of 4-hydroxyphenylboronic acid content on the microstructure, mesoporous properties, and electrochemical behavior of B-OMCs was further investigated.

2. Experimental section

2.1 Chemicals

Triblock polymer ($PEO_{106}PPO_{70}PEO_{106}$) provided by Sigma-Aldrich with an average M_w of 12 600. Formaldehyde (37 wt%), phenol, 4-hydroxyphenylboronic acid were obtained from Aladdin Industrial Corporation. All chemicals were used without further purification.

2.2 Synthesis of HPBPF and HPB-OMCs

As shown in Scheme 1, 4-hydroxyphenylboronic acid-modified phenolic resins (HPBPF) were synthesized as follows. After

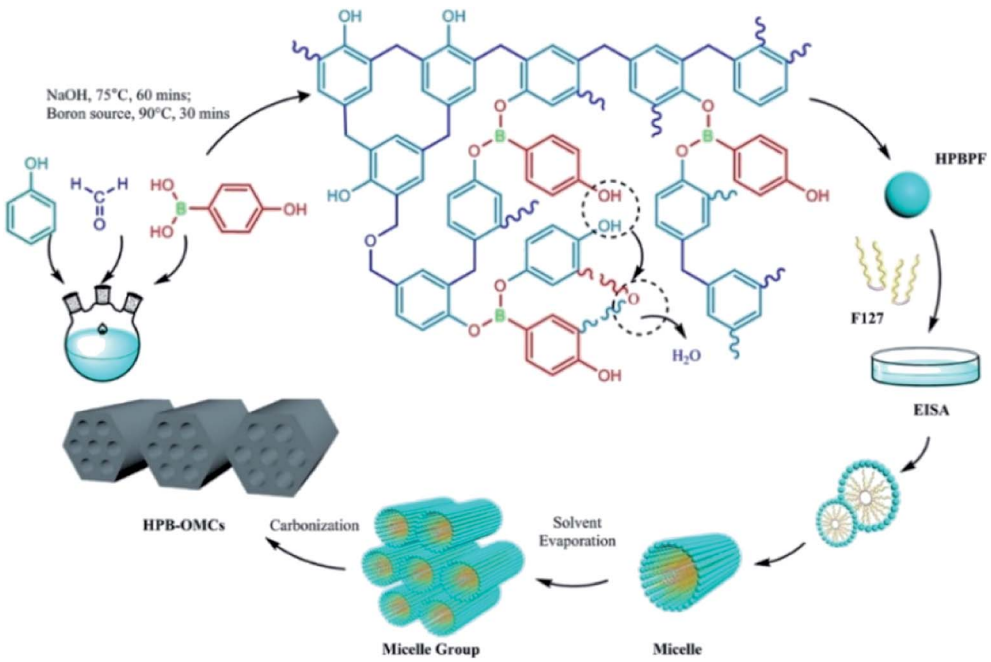

Scheme 1 Synthesis of 4-hydroxyphenylboronic acid-modified phenolic resins (HPBPF) and new boron-doped mesoporous carbon (HPB-OMCs).

polycondensation of phenol and formaldehyde (37 wt%) at 75 °C for 60 mins, a certain amount of 4-hydroxyphenylboronic acid was fed into the system and reacted at 90 °C for 30 mins to obtain the HPBPF precursor.

The new boron-doped mesoporous carbons (HPB-OMCs) were prepared with the HPBPF (precursor), F127 (template agent) and HCl (self-assembly regulator) *via* the EISA approach (evaporation at 25 °C for 36 h, curing at 100 °C for 18 h, and carbonized at 800 °C for 2 h in N_2 atmosphere as our previous research).[20] The obtained samples were named as *x*-HPB-OMCs ($x = 0, 0.05, 0.10, 0.15, 0.20$), where *x* denotes the mole ratio of 4-hydroxyphenylboronic acid and phenol.

Boric acid-modified phenolic resin (BPF, a mole ratio of boronic acid/phenol = 0.15), pure phenolic resin (PF) as well as the corresponding mesoporous carbons (B-OMC, OMC) were prepared in the same condition for comparison.

2.3 Characterization

Fourier transforms infrared (FTIR) analysis was performed from KBr pellets using a Nicolet 5700 spectrometer. Thermogravimetry (TG) was carried out on a NETZSCH TG 209C. X-ray photoelectron spectroscopy (XPS) was recorded using ESCALAB 250 at 150 W. Small angle X-ray powder diffraction (XRD) patterns were achieved on a Rigaku D/max-2550 with Cu-Kα as the radiation. The nitrogen adsorption–desorption isotherm was conducted on an ASAP 2020 (Micromeritics, USA). The specific surface area of the sample was calculated according to the Brunauer–Emmett–Teller method. And transmission electron microscopy (TEM) was operated on a JEM-1400 instrument.

2.4 Electrochemical measurements

The mixture of HPB-OMCs, acetylene black, and poly(tetrafluoroethylene) was pasted on a Ti mesh as an electrode with a weight ratio of 85 : 10 : 5. After dried overnight at 110 °C and impregnated by the electrolyte under vacuum, the experiments were carried out in a three-electrode system in the 1 M H_2SO_4 electrolyte with HPB-OMCs as the working electrode.

The cyclic voltammetry (CV) and the galvanostatic charge–discharge (GCD) measurements were conducted on the electrochemical workstation (CHI66D, China). The gravimetric capacitance of the sample was evaluated according to the equation $C_m = I\Delta t/(m\Delta U)$.

3. Results and discussion

3.1 Thermal stability of the precursors

Thermal stability, as well as the char yield of pure phenolic resins (PF), boronic acid-modified resins (BPF), and 4-hydroxyphenylboronic acid-modified resins (0.15-HPBPF), were further investigated by thermogravimetric analysis. As revealed in Fig. 1, the char yield of 0.15-HPBPF reaches 64.8%, much higher than those of BPF (62.8%) and PF (60.1%) at 1000 °C with the same molar amount of B source. According to the results of model calculations based on density functional theory (DFT), shorting the distance between phenol rings in the PF resin is conducive to the char formation during the pyrolysis.[26] The

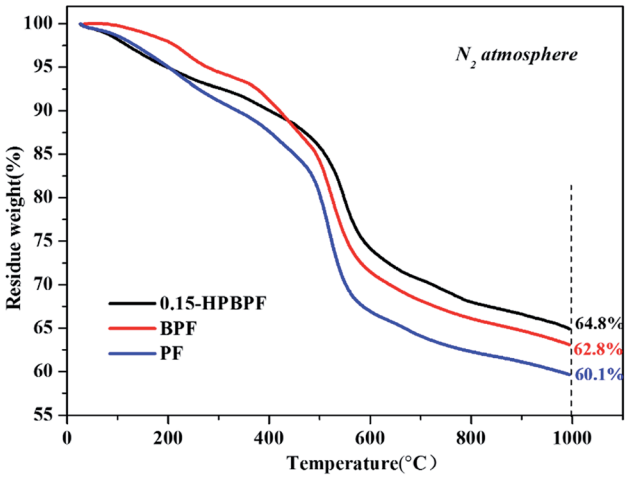

Fig. 1 Thermogravimetric analysis curves of the PF, BPF, and 0.15-HPBPF with a heating rate of 10 °C min^{-1} in N_2.

centroid distance between the two phenol rings in 0.15-HPBPF is closer than that in BPR. Moreover, the vulnerable active zone of HPBPF is partially transferred from borate structure to a much stable phenolic ring in this process.[27] The improvement of the thermal stability of HPBPF could reduce the shrinkage of char channels during carbonization. Meanwhile, the solubility of the resins in ethanol was also explored, and the results are given in Fig. S1, ESI.† The BPF resin cannot be dissolved in ethanol very well, leading to a cloudy solution. While the HPBPF shows excellent solubility in ethanol, in favor of achieving well-ordered self-assembles even with a high boron introduction.

3.2 Chemical structural characterization

The FT-IR spectra of OMC, B-OMC, and 0.15-HPB-OMC are displayed in Fig. 2. The absorption peaks at 1450 cm^{-1} and 1542 cm^{-1} correspond to the skeleton stretching vibration of the C=C bond of the benzene ring.[28] However, the intensity of

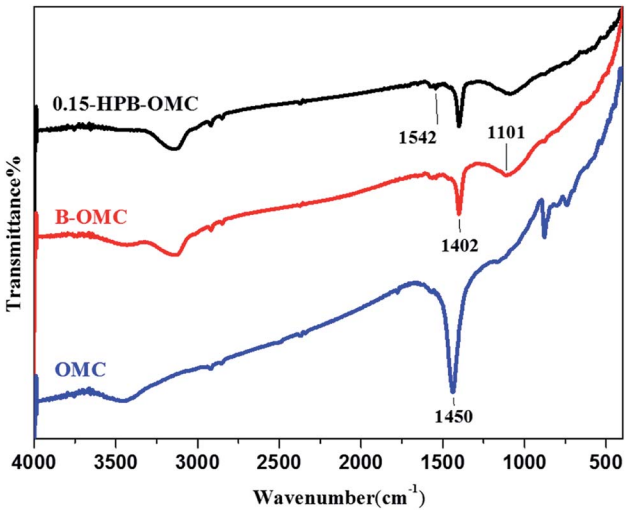

Fig. 2 FT-IR spectra of OMC, B-OMC, and 0.15-HPB-OMC.

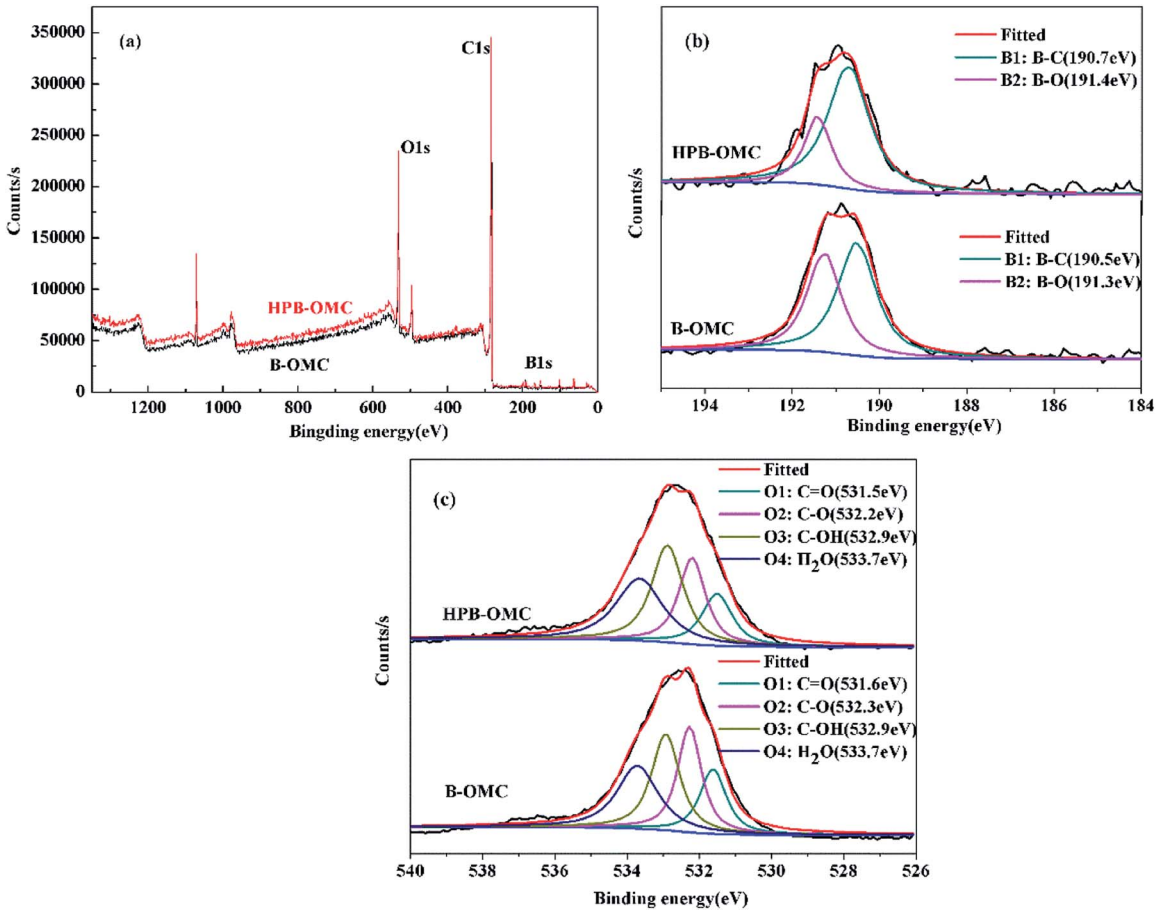

Fig. 3 XPS spectra of HPB-OMC and B-OMC (a), B 1s (b), O 1s (c).

the peak decreases because B atoms embedded in the carbon lattice at high temperatures destroyed the original carbon structure.[29] The peaks at 1101 cm^{-1} and 1402 cm^{-1} are attributed to the stretching vibration of B–C[30,31] and B–O triangular structure,[18,23] respectively. The results of FT-IR analysis demonstrate that boron atoms have been introduced into the lattice of carbon.

The formations of HPB-OMC and B-OMC were analyzed by XPS, and the results are presented in Fig. 3(b). The B 1s peak can be divided into the B–C (HPB-OMC: 190.7 eV, B-OMC: 190.5 eV) and B–O bond (HPB-OMC: 191.4 eV, B-OMC: 191.3 eV),[32–34] indicating that the boron is doped into the carbon backbone.[35] Meanwhile, the total B content of HPBPF is 3.96%, 1.61% higher than that of BPF. And the content of B–C (2.90%) in the HPB-OMC is almost three times of B–O content (1.05%), as listed in Table 2. The B–C bond could promote the oxidation–reduction reaction,[36] therefore, leading to better electrochemical performance and higher pseudo capacitance.

The O 1s spectrum in Fig. 3(c) could be fitted into four peaks, belonging to the bond of C=O (531.5 eV, 531.6 eV), C–O (532.2 eV,

Table 2 XPS analysis of HPB-OMC and B-OMC

	HPB-OMC		B-OMC	
Element	B. E. (eV)	Content (wt%)	B. E. (eV)	Content (wt%)
B	190.7 (B–C)	2.90	190.5 (B–C)	1.32
	191.4 (B–O)	1.05	191.3 (B–O)	1.03
Total content	—	3.96	—	2.35
O	531.5 (C=O)	3.87	531.6 (C=O)	4.96
	532.2 (C–O)	5.69	532.3 (C–O)	6.32
	532.9 (C–OH)	7.51	532.9 (C–OH)	7.83
	533.7 (H_2O)	7.09	533.7 (H_2O)	7.42
Total content	—	24.17	—	26.54

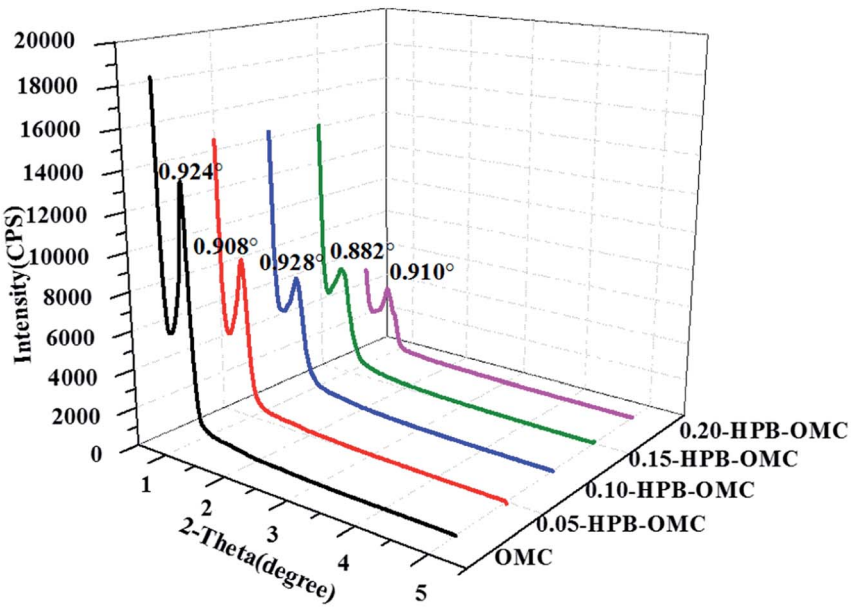

Fig. 4 Small-angle XRD patterns of HPB-OMCs.

532.3 eV), C–OH (532.9 eV, 532.9 eV), and H_2O (533.7 eV, 533.7 eV), respectively.[37] The O content of HPB-OMC is slightly lower than that of B-OMC. High oxygen content may increase the efficiency of capacitance retention at a high scan rate.[38]

3.3 Microstructure of HPB-OMCs

The SAXRD patterns of HPB-OMCs are displayed in Fig. 4. The diffraction peaks of OMC, 0.05-HPB-OMC, 0.10-HPB-OMC, 0.15-HPB-OMC, 0.20-HPB-OMC appeared at 0.924°, 0.908°,0.928°, 0.882°, and 0.910°, respectively, suggesting the well-ordered structure of HPB-OMCs.[38] The uncrosslinked phenolic hydroxyl of 4-hydroxyphenylboric acid not only improves the solubility of phenolic resins but also enhances the hydrogen bond interaction between the HPBPF and F127 during the self-assembly process, leading to a well-ordered mesoporous structure even with high boron content.

The interplanar spacing (d) of HPB-OMCs was calculated according to Bragg's Law: $2d \sin\theta = n\lambda$, and the results are listed in Table 3. The maximum value appears in 0.15-HPB-OMC, indicating the quite low channel shrinkage during calcination.

Also, all samples exhibit typical IV isotherms with well-defined H1 hysteresis loops at the position of relative pressure $P/P_0 = 0.4$ in Fig. 5(a), suggesting their mesoporous structure. However, the BET specific surface area and microspore volume of HPB-OMCs decrease gradually with the addition of 4-hydroxyphenylboronic acid.

In the previous report, the pore size distribution of B-OMCs usually gets broaden with the increase of the amount of boron doping.[15] It hardly changed for the samples of HPB-OMCs, as shown in Fig. 5(b). But the specific surface area of 0.20-HPB-OMC decreased. The possible reason may be the volatilization of the excess and unreacted boron source during carbonization partially destroyed the structure of OMCs, leading to some channel collapse. The 0.15-HPB-OMC owns the optimum comprehensive structural performance among all samples.

As the TEM images revealed in Fig. 6, all HPB-OMCs samples possess a two-dimensional hexagonal *P6mm* microstructure. Long 1D channels along the (100) direction and hexagonally arranged pores along the (001) direction are presented in the sample of 0.15-HPB-OMC. But the order degree and specific surface area of 0.20-HPB-OMC decrease a little for the slight structural collapse, which is consistent with the results of BET and XRD.

3.4 Electrochemical properties

Electrochemical properties of the electrodes based on HPB-OMCs with different boron-doped contents were evaluated. And GCD curves at the current density of 0.2 A g^{-1}, 1 A g^{-1}, and

Table 3 The structural properties, B contents and specific capacitance of *x*-HPB-OMCs

Sample	S_{BET}[a] (m^2 g^{-1})	S_{mic} (m^2 g^{-1})	V_t[b] (cm^3 g^{-1})	V_{mic} (cm^3 g^{-1})	D_p (nm)	d (nm)	B_{XPS}[c] (wt%)	C_p[d] (F g^{-1})
OMC	619.8	265.2	0.50	0.13	4.58	9.55	0	55
0.05-HPB-OMC	599.3	226.8	0.47	0.11	4.77	9.72	1.02	151
0.10-HPB-OMC	589.3	248.5	0.41	0.12	4.80	9.51	2.56	169
0.15-HPB-OMC	567.6	196.9	0.38	0.08	4.79	10.01	3.96	183
0.20-HPB-OMC	495.1	131.2	0.37	0.06	4.77	9.69	4.10	156

[a] Calculated by using the BET method. [b] Derived from the BJH method. [c] Determined by XPS. [d] Measured at the current density of 1 A g^{-1}.

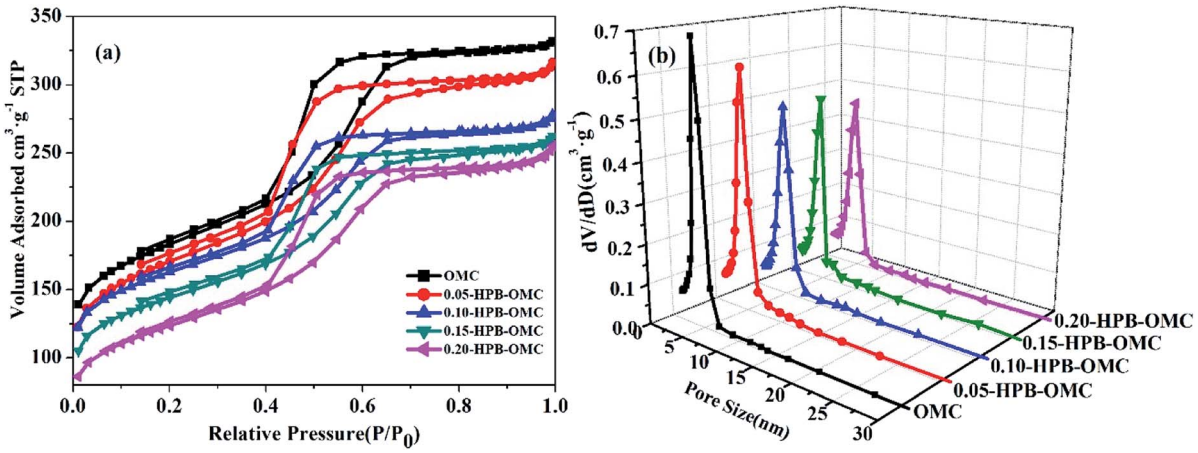

Fig. 5 (a) N_2 adsorption–desorption isotherms, and (b) pore size distributions of *x*-HPB-OMCs.

10 A g^{-1} are shown in the Fig. 7 and S2, in ESI.† The attenuation of the specific capacitance decreased as the current scanning density increases because transmission resistance of the electrolyte ions increased with current density in the channels. The isosceles triangle curves of all samples imply ideal double-layer capacitance behaviors.

With the increase of the B-doped amount, the specific capacitance of HPB-OMCs electrode raised from 55 F g^{-1} (OMC) to 183 F g^{-1} (0.15-HPB-OMC), 17.3% higher than that of B-OMCs (156 F g^{-1}) at a current density of 1 A g^{-1}.[19] Even at the high current density of 10 A g^{-1}, the capacitance of 0.15-HPB-OMC remains at 124 F g^{-1}, still much higher than the reported date.[39] As more boron atoms are embedded into the lattice of carbon, more anions in the electrolyte are attracted by the electron-deficient boron. The enhancement of the wettability between the electrode and electrolyte also leads to a high pseudo capacitance.[23,40]

All samples show nearly rectangular electrochemical curves in Fig. 8(a), meaning their typical electric double-layer capacitor behavior. The appearance of redox peaks in the voltage range of 0.3 to 0.5 V for all HPB-OMCs, which demonstrates the existence of reversible redox transitions when the samples are polarized.[41]

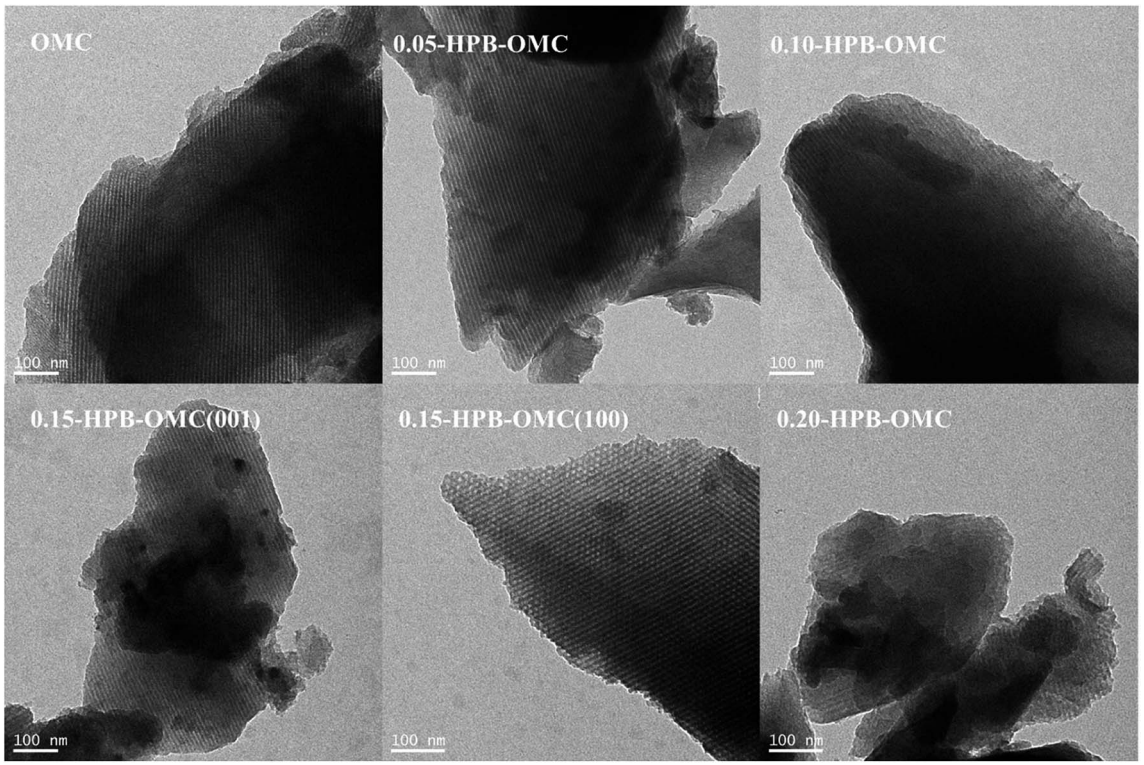

Fig. 6 TEM images of HPB-OMCs with the different mole ratios of 4-hydroxyphenylboronic acid and phenol.

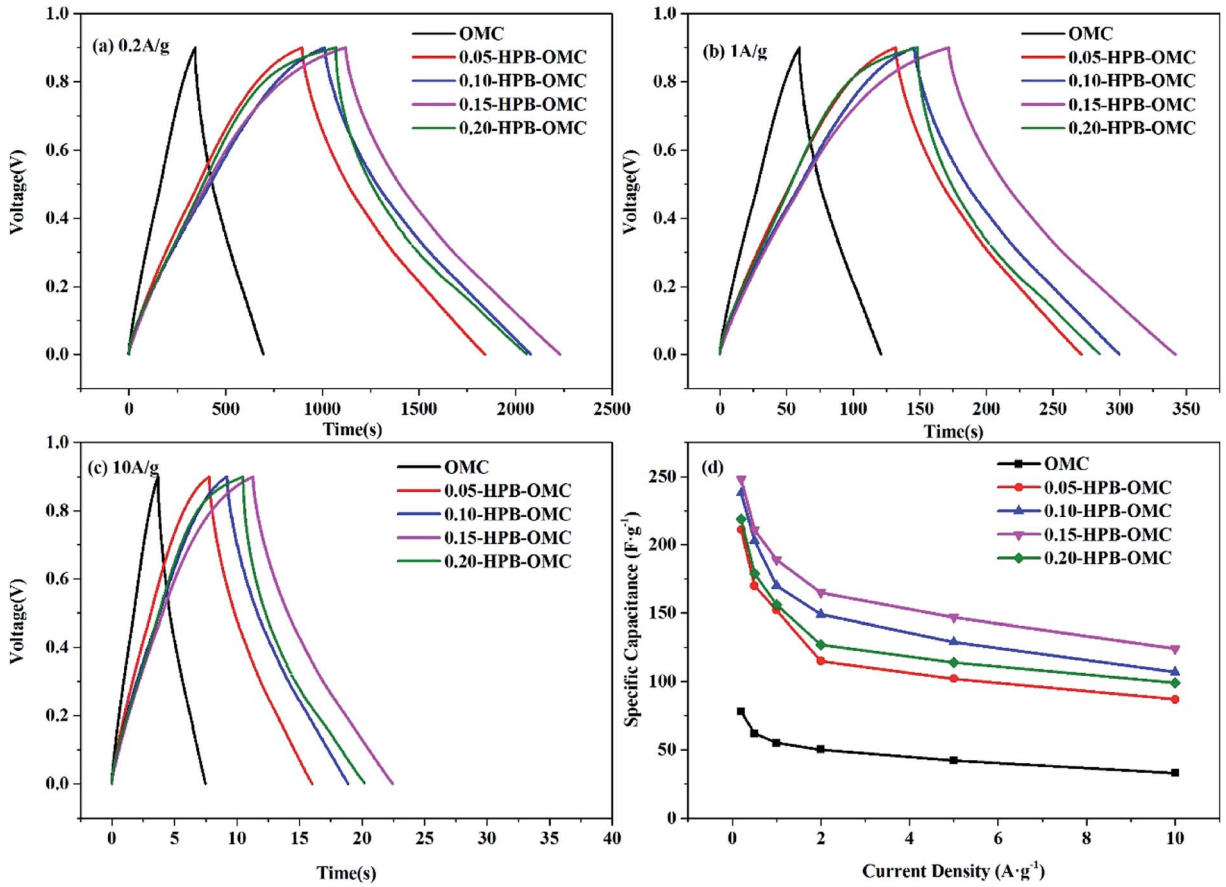

Fig. 7 GCD curves of the HPB-OMCs at a current density of 0.2 A g^{-1} (a), 1 A g^{-1} (b), 10 A g^{-1} (c), and specific capacitance of HPB-OMCs at different current density (d).

And the maximum response current (1.64 A g^{-1}) of 0.15-HPB-OMC shows its highest utilization of the active material.[42,43] For 0.20-HPB-OMC, however, the response current at scanning potential decreases, due to its relatively small specific surface area and partly being blocked ion transport channels.

CV curves of the 0.15-HPB-OMC sample at a scan rate from the 5 mV s^{-1} to 100 mV s^{-1} are displayed in Fig. 8(b). They retain nearly rectangular shape even at a high scan rate of 100 mV s^{-1}. With the increase of scanning rate, both oxidation/reduction current and transport rate of electrolyte ions in the mesoporous channel raise gradually. But channel defect is magnified with the increase of scanning rate at the same time, resulting in a slight distortion of the rectangle.[44]

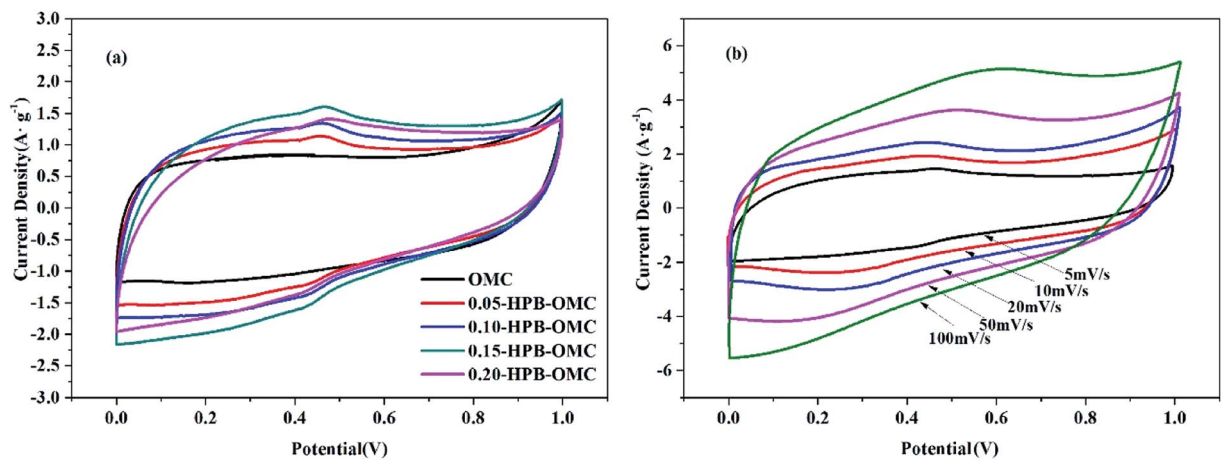

Fig. 8 CV curves of various HPB-OMCs at a scan rate of 5 mV s^{-1} (a) and CV curves of 0.15-HPB-OMC at different scan rate (b).

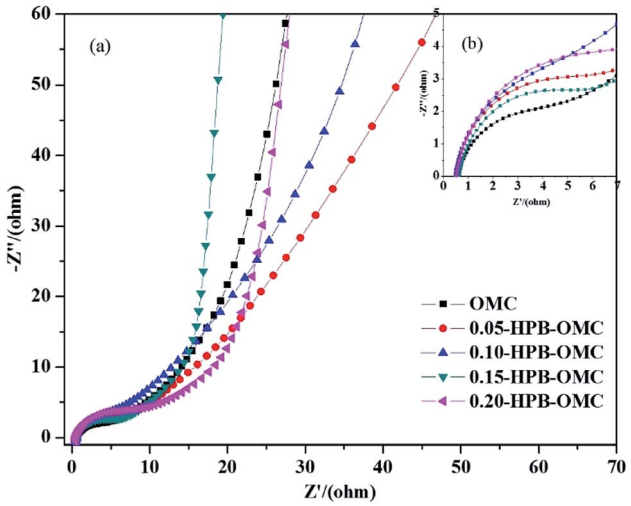

Fig. 9 (a) Nyquist plots of HPB-OMCs and (b) the enlargement at high frequency region.

Boron-doping could improve the wettability between the surface of carbonaceous materials and the electrolyte, bring about a relatively small transfer impedance of electrons, and provide a fast-moving channel for ion transmission.[45] In Nyquist plots shown in Fig. 9, the radius of the semicircle at high frequency reflects charge transfer resistance, and the slope of the oblique line represents Warburg diffusion resistance, respectively.[46] Compared with others, the much smaller semicircle of 0.15-HPB-OMC at high frequency shows its lower ion transportation resistance, and the almost vertical oblique line indicates it an ideal double-layer supercapacitor at low frequency. The sample of 0.15-HPB-OMC exhibits superior electrochemical performances.

Besides, the intercept from the beginning of semicircle at high frequency region to the origin in Fig. 9(b) represents the equivalent series resistance of the electrode. It is almost same for all samples, which suggests that no extra internal resistance is produced by boron doping for HPB-OMCs.[47]

4. Conclusion

The high B-doped ordered mesoporous carbon (HPB-OMC) was prepared by using 4-hydroxyphenylboronic acid-modified phenolic resin (HPBPF) as boron and carbon precursor *via* the evaporation-induced self-assembly approach. The as-prepared HPB-OMC has relatively high BET surface areas (567.6 $m^2 g^{-1}$), suitable pore size (4.8 nm), and uniformly distributed channel. Both solubility of the resins in ethanol and thermal stability of the pore structure during carbonization are improved. As an electrode material, the 0.15-HPB-OMC possesses excellent electrochemical performances and the highest specific capacitance of 183 F g^{-1} at the current density of 1 A g^{-1}, which are 17% higher than that of B-OMC 156 F g^{-1}.

Conflicts of interest

There are no conflicts to declare.

Acknowledgements

This research was supported by the National Natural Science Foundation of China (51303054) and Fundamental Research Funds for the Central Universities (50321041917001).

References

1 J. Xu, L. Z. Wen, Y. L. Gan and B. Xue, *Mol. Catal.*, 2020, **485**, 110848.
2 J. Goscianska, R. Pietrzak and J. Matos, *Catal. Today*, 2018, **301**, 204–216.
3 S. Khan, R. P. Raj, T. V. R. Mohan, S. Bhuvaneswari, U. V. Varadaraju and P. Selvam, *J. Electroanal. Chem.*, 2019, **848**, 113242.
4 F. Wu, J. Qian, W. Wu, Y. Ye, Z. Sun, B. Xu, X. Yang, Y. Xu, J. Zhang and R. Chen, *Nano Res.*, 2017, **10**, 426–436.
5 X. Zhao, A. Wang, J. Yan, G. Sun, L. Sun and T. Zhang, *Chem. Mater.*, 2010, **22**, 5463–5473.
6 F. Cheng, X. Yang, S. Zhang and W. Lu, *J. Power Sources*, 2020, **450**, 227678.
7 M. Li, K. Huang, J. A. Schott, Z. Wu and S. Dai, *Microporous Mesoporous Mater.*, 2017, **249**, 34–41.
8 A. F. M. EL-Mahdy, T. E. Liu and S. W. Kuo, *J. Hazard. Mater.*, 2020, **391**, 122163.
9 C. He and X. Hu, *Ind. Eng. Chem. Res.*, 2011, **50**, 14070–14083.
10 X. Bo and L. Guo, *Phys. Chem. Chem. Phys.*, 2013, **15**, 2459–2465.
11 J. Wu, Z. Yang, Q. Sun, X. Li, P. Strasser and R. Yang, *Electrochim. Acta*, 2014, **127**, 53–60.
12 D. H. Zhong, H. Sano, Y. Uchiyama and K. Kobayashi, *Carbon*, 2000, **38**, 1199–1206.
13 L. R. Radovic, M. Karra, K. Skokova and P. A. Thrower, *Carbon*, 1998, **36**, 1841–1854.
14 H. I. Lee, J. H. Kim, D. J. You, J. E. Lee, J. M. Kim, W. S. Ahn, C. Pak, S. H. Joo, H. Chang and D. Seung, *Adv. Mater.*, 2008, **20**, 757–762.
15 H. J. Lu, Y. Li, L. Q. Zhang, H. N. Li, Z. X. Zhou, A. R. Liu, Y. J. Zhang and S. Q. Liu, *RSC Adv.*, 2015, **5**, 52126–52131.
16 X. Zhao, Q. Zhang, B. Zhang, C. M. Chen, J. Xu, A. Wang, D. S. Su and T. Zhang, *RSC Adv.*, 2013, **3**, 3578.
17 K. Zeng, J. Su, X. Cao, X. Zheng, X. Li, J. H. Tian, C. Jin and R. Yang, *J. Alloys Compd.*, 2020, **824**, 153908.
18 D. W. Wang, F. Li, Z. G. Chen, G. Q. Lu and H. M. Cheng, *Chem. Mater.*, 2008, **20**, 7195–7200.
19 M. Enterría, M. F. R. Pereira, J. I. Martins and J. L. Figueiredo, *Carbon*, 2015, **95**, 72–83.
20 J. Song, Y. Zhang and Y. Liu, *RSC Adv.*, 2015, **5**, 20734–20740.
21 J. Su, X. Cao, J. Wu, C. Jin, J. H. Tian and R. Yang, *RSC Adv.*, 2016, **6**, 24728–24737.
22 Y. Zhang, W. Dai, Y. Liu and B. Ma, *RSC Adv.*, 2017, **7**, 8250–8257.
23 X. Zhai, Y. Song, J. Liu, P. Li, M. Zhong, C. Ma, H. Wang, Q. Guo and L. Zhi, *J. Electrochem. Soc.*, 2012, **159**, E177–E182.
24 S. Wang, X. Jing, Y. Wang and J. Si, *Polym. Adv. Technol.*, 2014, **25**, 152–159.

25 L. Yang, S. Jiang, Y. Zhao, L. Zhu, S. Chen, X. Wang, Q. Wu, J. Ma, Y. Ma and Z. Hu, *Angew. Chem., Int. Ed.*, 2011, **50**, 7132–7135.
26 C. Bian, Y. Wang, S. Wang, Y. Zhong, Y. Liu and X. Jing, *Polym. Degrad. Stab.*, 2015, **119**, 190–197.
27 C. Martín, J. C. Ronda and V. Cádiz, *J. Polym. Sci., Part A: Polym. Chem.*, 2006, **44**, 3503–3512.
28 S. Wang, Y. Wang, C. Bian, Y. Zhong and X. Jing, *Appl. Surf. Sci.*, 2015, **331**, 519–529.
29 S. Wang, X. Xing, J. Li and X. Jing, *Appl. Surf. Sci.*, 2018, **428**, 912–923.
30 M. G. Rodriguez, O. V. Kharissova and U. O. Mendez, *Rev. Adv. Mater. Sci.*, 2004, **7**, 55–60.
31 T. V. Khai, H. G. Na, D. S. Kwak, Y. J. Kwon, H. Ham, K. B. Shim and H. W. Kim, *Chem. Eng. J.*, 2012, **211–212**, 369–377.
32 Z. F. Zhou, I. Bello, M. K. Lei, K. Y. Li, C. S. Lee and S. T. Lee, *Surf. Coat. Technol.*, 2000, **128–129**, 334–340.
33 M. O. Watanabe, T. Sasaki, S. Itoh and K. Mizushima, *Thin Solid Films*, 1996, **281–282**, 334–336.
34 A. Perrone, A. P. Caricato, A. Luches, M. Dinescu, C. Ghica, V. Sandu and A. Andrei, *Appl. Surf. Sci.*, 1998, **133**, 239–242.
35 S. Ding, S. Zheng, M. Xie, L. Peng, X. Guo and W. Ding, *Microporous Mesoporous Mater.*, 2011, **142**, 609–613.
36 C. Wang, Z. Guo, W. Shen, Q. Xu, H. Liu and Y. Wang, *Adv. Funct. Mater.*, 2014, **24**, 5511–5521.
37 S. D. Gardner, C. S. K. Singamsetty, G. L. Booth and G. He, *Carbon*, 1995, **33**, 587–595.
38 T. Kwon, H. Nishihara, H. Itoi, Q. H. Yang and T. Kyotani, *Langmuir*, 2009, **25**, 11961–11968.
39 Y. Zhang, B. E. Ma and Y. Liu, *RSC Adv.*, 2018, **8**, 17629–17634.
40 H. Guo and Q. Gao, *J. Power Sources*, 2009, **186**, 551–556.
41 C. O. Ania, V. Khomenko, E. Raymundo-Piñero, J. B. Parra and F. Béguin, *Adv. Funct. Mater.*, 2007, **17**, 1828–1836.
42 G. Qu, J. Cheng, X. Li, D. Yuan, P. Chen, X. Chen, B. Wang and H. Peng, *Adv. Mater.*, 2016, **28**, 3646–3652.
43 L. Li, E. Liu, J. Li, Y. Yang, H. Shen, Z. Huang, X. Xiang and W. Li, *J. Power Sources*, 2010, **195**, 1516–1521.
44 Y. Liu, Z. Wang, W. Teng, H. Zhu, J. Wang, A. A. Elzatahry, D. Al-Dahyan, W. Li, Y. Deng and D. Zhao, *J. Mater. Chem. A*, 2018, **6**, 3162–3170.
45 H. K. Song, Y. H. Jung, K. H. Lee and L. H. Dao, *Electrochim. Acta*, 1999, **44**, 3513–3519.
46 X. Zhou, J. Xu, W. Zhu, X. Wang, Z. Liu, N. Yuan and J. Ding, *Mater. Lett.*, 2017, **204**, 177–180.
47 C. Guan, X. Liu, W. Ren, X. Li, C. Cheng and J. Wang, *Adv. Energy Mater.*, 2017, **7**, 1602391.

